(12) LEVEL

AD

A 083889

TECHNICAL REPORT ARBRL-TR-02225

ANALYTICAL MODELS FOR THE COMPRESSIVE HEATING IGNITION OF HIGH EXPLOSIVES

John Starkenberg

March 1980

US ARMY ARMAMENT RESEARCH AND DEVELOPMENT COMMAND
BALLISTIC RESEARCH LABORATORY
ABERDEEN PROVING GROUND, MARYLAND

Destroy this report when it is no longer needed.
Do not return it to the originator.

Secondary distribution of this report by originating or sponsoring activity is prohibited.

Additional copies of this report may be obtained from the National Technical Information Service, U.S. Department of Commerce, Springfield, Virginia 22151.

The findings in this report are not to be construed as an official Department of the Army position, unless so designated by other authorized documents.

The use of trade names or manufacturers' names in this report does not constitute indorsement of any commercial product.

UNCLASSIFIED
SECURITY CLASSIFICATION OF THIS PAGE (When Data Entered)

REPORT DOCUMENTATION PAGE	READ INSTRUCTIONS BEFORE COMPLETING FORM
1. REPORT NUMBER TECHNICAL REPORT ARBRL-TR-02225	2. GOVT ACCESSION NO. AD-A083 889	3. RECIPIENT'S CATALOG NUMBER
4. TITLE (and Subtitle) ANALYTICAL MODELS FOR THE COMPRESSIVE HEATING IGNITION OF HIGH EXPLOSIVES		5. TYPE OF REPORT & PERIOD COVERED Final 6. PERFORMING ORG. REPORT NUMBER
7. AUTHOR(s) John Starkenberg		8. CONTRACT OR GRANT NUMBER(s)
9. PERFORMING ORGANIZATION NAME AND ADDRESS US Army Armament Research and Development Command Ballistic Research Laboratory (ATTN: DRDAR-BLT) Aberdeen Proving Ground, MD 21005		10. PROGRAM ELEMENT, PROJECT, TASK AREA & WORK UNIT NUMBERS 1L161102AH60
11. CONTROLLING OFFICE NAME AND ADDRESS U.S. Army Armament Research & Development Command U.S. Army Ballistic Research Laboratory (ATTN: DRDAR-BL) Aberdeen Proving Ground, MD 21005		12. REPORT DATE MARCH 1980 13. NUMBER OF PAGES 44
14. MONITORING AGENCY NAME & ADDRESS(if different from Controlling Office)		15. SECURITY CLASS. (of this report) UNCLASSIFIED 15a. DECLASSIFICATION/DOWNGRADING SCHEDULE

16. DISTRIBUTION STATEMENT (of this Report)

Approved for public release, distribution unlimited.

17. DISTRIBUTION STATEMENT (of the abstract entered in Block 20, if different from Report)

18. SUPPLEMENTARY NOTES

19. KEY WORDS (Continue on reverse side if necessary and identify by block number)

adiabatic compression, compressive heating, ignition, setback, sensitivity

20. ABSTRACT (Continue on reverse side if necessary and identify by block number) (blk)

Two one-dimensional models to predict the temperature history of an explosive surface subject to compressive heating from the rapid collapse of an adjacent air layer are reported herein. Computations made using the more sophisticated finite compression-rate model show qualitative agreement with the experimental behavior while results obtained from the simpler adiabatic compression model are sometimes misleading. The most important observation is that planar one-dimensional gap closure cannot explain ignition as observed in experiments. Several multidimensional effects have been introduced into the

DD FORM 1 JAN 73 1473 EDITION OF 1 NOV 65 IS OBSOLETE

UNCLASSIFIED
SECURITY CLASSIFICATION OF THIS PAGE (When Data Entered)

models. The results show that enhanced energy transport caused by convection and turbulence must be present in conjunction with rapid local pressurization and/or convergent air-flow, unless the enhancement is confined to a boundary layer adjacent to the explosive. In addition, the dieseling mechanism of sensitization has been considered indicating that explosive particle sizes small enough to exhibit increased temperature may be present.

TABLE OF CONTENTS

LIST OF ILLUSTRATIONS

LIST OF TABLES

I. INTRODUCTION

Compressive heating caused by the rapid collapse of an air layer adjacent to a high explosive material has been implicated as a mechanism of ignition under artillery setback conditions. This conclusion has been reached as a result of activator experiments conducted at the Ballistic Research Laboratory (BRL)[1]. The activator is an experimental apparatus in which an air gap adjacent to a high explosive sample is rapidly compressed by a piston. In support of these experiments, two one-dimensional models have been developed to trace the thermal history of the explosive sample, the air gap and the piston.

The apparatus, illustrated schematically in Figure 1, consists of a heavy confinement cylinder with a 12.7mm bore enclosing the explosive sample, a driving piston and a backup piston. The driving piston is

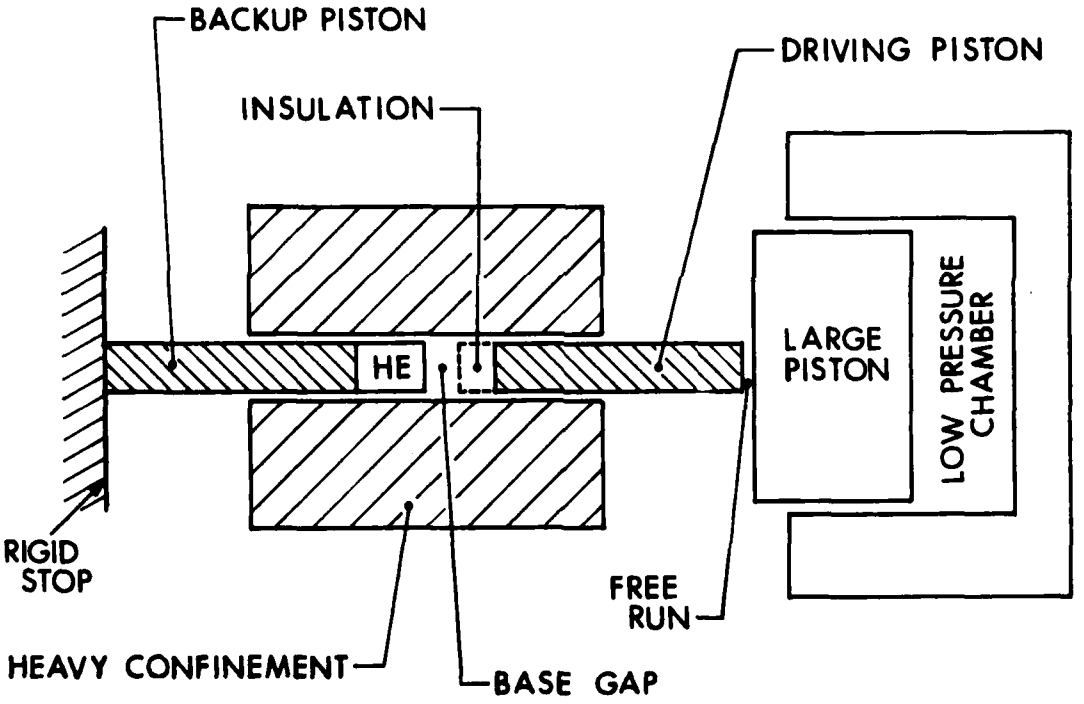

Figure 1. Activator Schematic

[1] *Taylor, B., C., Starkenberg, J., and Ervin, L. H.; "An Experimental Investigation of Composition B Ignition under Artillery Setback Conditions, BRL Report to be published.*

set in motion by a larger piston which is in turn driven by a propellant burned in a low pressure chamber or breech. The backup piston rests against a rigid stop. An air gap is set between the explosive and the driving piston and an additional free run gap may be allowed between the driving and the large piston. The explosive sample is heated as the air gap is compressed. The sum of the air gap thickness and the free run is referred to as the total run. In order to control the gap closure rate, shear pins are used to allow the breech to pressurize before the large piston begins to accelerate. Thus the pressurization rate and peak pressure depend on propellant charge design, total run and shear pin strength. It is further possible to pressurize or evacuate the air gap and to use various insulating materials at the face of the driving piston.

The experimental evidence to-date indicates that the sensitivity of the explosive to violent reaction is governed by a number of factors. Specifically these are:

1. total run
2. peak pressure
3. pressurization rate
4. initial air gap thickness
5. initial air pressure
6. piston thermal conductivity
7. air leakage
8. state of the explosive surface

In the experiments conducted thus far the first three of the above were not varied independently. The list does not exhaust all possible influencing factors. The present study addresses all but the last of these.

A preliminary and final model have been constructed. For the preliminary model the air gap is assumed to be instantaneously compressed to its peak pressure and temperature. It is then possible to compute the temperature of the explosive-air interface, which is the parameter used for ranking the sensitivity of various configurations in this study. This model corresponds to an intuitive approach to the problem referred to as adiabatic compression which has been widely used to describe compressive heating. This concept is inappropriate when applied to the entire problem since it identifies only a limiting case which is incomplete and can be misleading. In order to more completely describe the situation a model in which the air gap is compressed at a finite rate is required. In this more sophisticated model, the heat equation is solved numerically for the temperature distribution in the three layers as a function of time. Compressive heating is introduced through a source term active in the air layer. The peak explosive-air interface temperature is extracted from these computations. An implicit finite difference scheme has been employed because of its flexibility and applicability to parabolic problems. The adiabatic compression model may be regarded as the limiting case for infinite pressurization rates.

The objective of the modeling is to treat the ignition problem by examining the effects of stimulus variations on sensitivity in order to verify the compressive heating hypothesis and to qualitatively predict activator behavior. A qualitative approach is necessary because the models are limited by their one-dimensional property while events occurring in the activator and in artillery ammunition are multidimensional in nature. Steps have been taken to account for some of the multidimensional aspects of the problem.

II. MODELING

A. Adiabatic Compression Model

As a first step consider the situation that arises when the air gap is instantaneously compressed from a known initial pressure to a known final pressure. Assuming that the air is an ideal polytropic gas results in the following expression for final air temperature, density and gap thickness.

$$\frac{\bar{T}_f}{\bar{T}_i} = \left(\frac{\bar{p}_f}{\bar{p}_i}\right)^{\frac{\gamma-1}{\gamma}}$$

$$\frac{\bar{\rho}_f}{\bar{\rho}_i} = \frac{\bar{\delta}_i}{\bar{\delta}_f} = \left(\frac{\bar{p}_f}{\bar{p}_i}\right)^{1/\gamma}$$

The temperature profile immediately after compression is in the form of a step with ambient temperature persisting in the explosive and the elevated temperature, $\bar{T}_f$, in the air. In this case the highest temperature arising in the explosive is the explosive-air interface temperature. This can be calculated using a solution to the heat equation for two semi-infinite layers instantaneously brought into contact following Carslaw and Jaeger[2]. The resulting expression for interface temperature is independent of time.

$$\frac{\bar{T}_{I\infty}}{\bar{T}_i} = 1 + \frac{\alpha}{1+\alpha}\left(\frac{\bar{T}_f}{\bar{T}_i} - 1\right) = 1 + \frac{\alpha}{1+\alpha}\left[\left(\frac{\bar{p}_f}{\bar{p}_i}\right)^{\frac{\gamma-1}{\gamma}} - 1\right]$$

---

[2] *Carslaw, H. S. and Jaeger, J. C.; Conduction of Heat in Solids, 2nd ed., Oxford University Press, 1959, pp 87 - 88.*

where

$$\alpha = \left(\frac{\bar{\rho}_f \, \bar{c}_{p_{air}} \, \bar{\kappa}_{air}}{\bar{\rho}_{he} \, \bar{c}_{p_{he}} \, \bar{\kappa}_{he}} \right)^{1/2}$$

The following expression for the ratio of the increase in interface temperature to the increase in air temperature may be generated.

$$\frac{\bar{T}_{I\infty} - \bar{T}_i}{\bar{T}_f - \bar{T}_i} = \frac{\Delta\bar{T}_{I\infty}}{\Delta\bar{T}_f} = \frac{\alpha}{1+\alpha} = \beta$$

This is referred to as the heating efficiency of the gas with respect to the explosive. Furthermore, α is a function of the final temperature and density of the air and thus of the compression ratio, $\bar{p}_f/\bar{p}_i$, and the initial state of the air before compression. It is possible, then, to predict the interface temperature knowing the compression ratio and the properties of the explosive and the air.

$$\frac{\bar{T}_{I\infty}}{\bar{T}_i} = 1 + \frac{\alpha_i \left(\frac{\bar{p}_f}{\bar{p}_i} \right)^{1/2\gamma} \left[\left(\frac{\bar{p}_f}{\bar{p}_i} \right)^{\frac{\gamma-1}{\gamma}} - 1 \right]}{1 + \alpha_i \left(\frac{\bar{p}_f}{\bar{p}_i} \right)^{1/2\gamma}} \qquad (1)$$

with

$$\alpha = \left[\frac{\bar{\rho}_i \, \bar{c}_{p_{air}} \, \bar{\kappa}_{air}}{\bar{\rho}_{he} \, \bar{c}_{p_{he}} \, \bar{\kappa}_{he}} \left(\frac{p_f}{p_i} \right)^{1/\gamma} \right]^{1/2} = \alpha_i \left(\frac{\bar{p}_f}{\bar{p}_i} \right)^{1/2\gamma}$$

This model excludes effects of pressurization rate, gap thickness, piston insulating capacity, and mass addition or leakage; these are studied by means of the more sophisticated model. A slightly more detailed approach which utilizes a solution to the heat equation for all three layers could be used. In this event the same initial interface temperature should be predicted since for sufficiently early times after compression even a very thin air layer will act as though infinite. At later times

the effect of the third layer would be to reduce the interface temperature. Thus the same maximum interface temperature is predicted and no additional information is generated through this approach.

B. Finite Compression-Rate Model

1. Governing Equations. The heat equation is applied in three layers consisting of the explosive, the air gap and the piston, illustrated in Figure 2. It takes a slightly different form in each of the layers. An Eulerian representation has been used.

Explosive (n=1)

$$\frac{D\bar{T}}{D\bar{t}} = \frac{1}{\bar{c}_p}\left[\frac{1}{\bar{\rho}}\frac{\partial}{\partial\bar{x}}\left(\bar{\kappa}\frac{\partial\bar{T}}{\partial\bar{x}}\right) + \bar{J}\right]$$

Air (n=2)

$$\frac{D\bar{T}}{D\bar{t}} = \frac{1}{\bar{\rho}\,\bar{c}_p}\left[\frac{\partial}{\partial\bar{x}}\left(\bar{\kappa}\frac{\partial\bar{T}}{\partial\bar{x}}\right) + \frac{D\bar{p}}{D\bar{t}}\right]$$

Piston (n=3)

$$\frac{D\bar{T}}{D\bar{t}} = \frac{1}{\bar{\rho}\,\bar{c}_p}\frac{\partial}{\partial\bar{x}}\left(\bar{\kappa}\frac{\partial\bar{T}}{\partial\bar{x}}\right)$$

Here

$$\frac{D}{D\bar{t}} = \frac{\partial}{\partial\bar{t}} + \bar{u}\frac{\partial}{\partial\bar{x}}$$

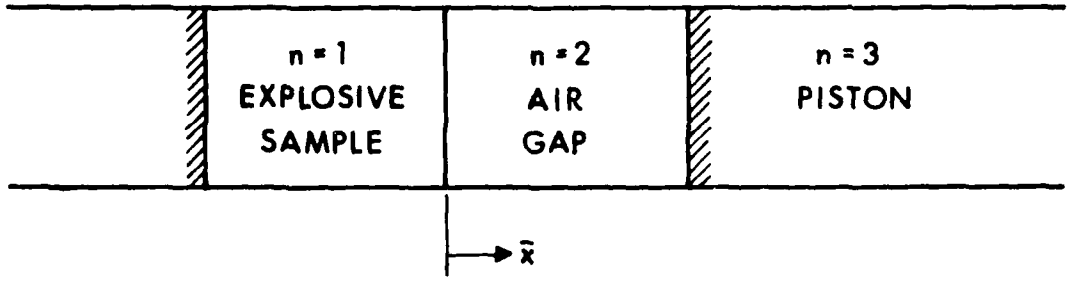

Figure 2. Finite Compression-Rate Model Schematic

is the particle derivative and $\bar{J}$ represents heating due to chemical reaction in the explosive. The equations may be generalized as follows:

$$\frac{D\bar{T}}{D\bar{t}} = \frac{1}{\bar{c}_p}\left\{\frac{1}{\bar{\rho}}\left[\frac{\partial}{\partial\bar{x}}\left(\bar{\kappa}\ \frac{\partial\bar{T}}{\partial\bar{x}}\right) + a_1\ \frac{D\bar{p}}{D\bar{t}}\right] + a_2\ \bar{J}\right\}$$

where

$$(a_1, a_2) = \begin{cases} (0,1) & \text{explosive} \\ (1,0) & \text{air} \\ (0,0) & \text{piston} \end{cases}$$

It is assumed that dissipation may be neglected in the air layer. The following additional assumptions are used in order to compute conditions in the air layer:

1. air pressure is uniform throughout the gap and varies with time in a prescribed manner
2. the ideal gas equation of state applies
3. velocity varies linearly in the air layer
4. thermal conductivity is constant in the explosive and piston and is a given function of temperature in the air layer

The first assumption implies that the pressurization is sufficiently slow to allow wave propagation through the entire air layer during a small increase in pressure. The consequences of assuming a linear velocity/ profile are discussed in the appendix. Note that constant density and specific heat are not implied. With these assumptions the general equation becomes

$$\frac{\partial\bar{T}}{\partial\bar{t}} + \bar{u}\ \frac{\partial\bar{T}}{\partial\bar{x}} = \frac{1}{\bar{c}_p}\left\{\frac{1}{\bar{\rho}}\left[\frac{\partial}{\partial\bar{x}}\left(\bar{\kappa}\ \frac{\partial\bar{T}}{\partial\bar{x}}\right) + a_1\ \frac{d\bar{p}}{d\bar{t}}\right] + a_2\ \bar{J}\right\}$$

In order to handle the compression of the air layer an expression for the total mass per unit area of the air in the gap at any time is used

$$\bar{m} = \int_{\bar{x}_\ell}^{\bar{x}_r} \bar{\rho}\, d\bar{x}$$

To account for leakage or mass addition during piston closure, $\bar{m}$ may be regarded as a function of time.

The ideal gas equation of state is used to relate density to pressure and temperature.

$$\bar{m} = \int_{\bar{x}_\ell}^{\bar{x}_r} \frac{\bar{p}}{\bar{R}_{air}\bar{T}} \, d\bar{x}$$

Since pressure is assumed uniform

$$\bar{m} = \frac{\bar{p}}{\bar{R}_{air}} \int_{\bar{x}_\ell}^{\bar{x}_r} \frac{d\bar{x}}{\bar{T}}$$

This expression relates the pressure, temperature profile and gap thickness at any instant.

The particle velocity, $\bar{u}$, vanishes in the explosive, varies linearly in the air and is uniform in the piston at any time.

$$\bar{u} = \begin{cases} 0 & \text{explosive} \\ \dfrac{\bar{x}-\bar{x}_\ell}{\bar{x}_r-\bar{x}_\ell}\,\bar{u}_p & \text{air} \\ \bar{u}_p & \text{piston} \end{cases}$$

The thermal conductivity of air is given by

$$\bar{\kappa}_{air} = \bar{C}_1 \bar{T}^{1/2} - \bar{C}_2 \qquad (3)$$

The values of $\bar{C}_1$ and $\bar{C}_2$ were obtained by fitting to data found in reference 3 and yield an accuracy of 5 percent between 300K and 400K and 2 percent between 400K and 1500K. This covers the entire range of gas temperatures encountered. The effect of pressure has been neglected.

2. Boundary Conditions: At interior boundaries (those between layers) temperature and heat flux are continuous.

---

[3] *National Bureau of Standards, Tables of Thermal Properties of Gases, Circular 546, 1955.*

$$\bar{T}_r^{n-1} = \bar{T}_\ell^{n} \qquad n=2,3$$

$$\bar{\kappa}_r^{n} \left(\frac{\partial \bar{T}}{\partial \bar{x}}\right)_r^{n} = \bar{\kappa}_\ell^{n+1} \left(\frac{\partial \bar{T}}{\partial \bar{x}}\right)_\ell^{n+1} \qquad n=1,2$$

where the superscript identifies the layer. At each exterior boundary (extreme left or right) either temperature or heat flux may be specified as a function of time.

left: $\bar{T}(\bar{t}, \bar{x}_\ell^{(1)}) = \bar{T}_L(\bar{t})$ or $\bar{\kappa}_{he} \frac{\partial \bar{T}}{\partial \bar{x}}(\bar{t}, \bar{x}_\ell^{(1)}) = \bar{Q}_L(\bar{t})$

right: $\bar{T}(\bar{t}, \bar{x}_r^{(3)}) = \bar{T}_R(\bar{t})$ or $\bar{\kappa}_p \frac{\partial \bar{T}}{\partial \bar{x}}(\bar{t}, \bar{x}_r^{(3)}) = \bar{Q}_R(\bar{t})$

3. Boundary Motion. The explosive-air interface is assumed to lie at a fixed point so that

$$\bar{U}_r^{(1)} = \bar{U}_\ell^{(2)} = 0$$

The air-piston interface moves at the piston velocity

$$\bar{U}_r^{(2)} = \bar{U}_\ell^{(3)} = \bar{u}_p$$

and the left and right exterior boundaries advance through the explosive and the piston respectively in order to move with the heated region in each layer. This spreads the temperature variation over the portion of the layer considered at any time and leads to more accurate computations.

$$\bar{U}_\ell^{(1)} = \frac{-5}{2}\left(\frac{\bar{\kappa}_{he}}{\bar{\rho}_{he}\,\bar{c}_{p_{he}}\,\bar{t}}\right)^{1/2}$$

$$\bar{U}_r^{(3)} = \bar{u}_p + \frac{5}{2}\left(\frac{\bar{\kappa}_p}{\bar{\rho}_p\,\bar{c}_{p_p}\,\bar{t}}\right)^{1/2}$$

The boundary positions are then given by

$$\bar{x}_\ell^{(1)} = -5\left(\frac{\bar{\kappa}_{he}\bar{t}}{\bar{\rho}_{he}\,\bar{c}_{p_{he}}}\right)^{1/2} \tag{4}$$

$$\bar{x}_r^{(1)} = \bar{x}_\ell^{(2)} = 0$$

$$\bar{x}_r^{(2)} = \bar{x}_\ell^{(3)} = \bar{\delta}$$

$$\bar{x}_r^{(3)} = \bar{\delta} + 5\left(\frac{\bar{\kappa}_p\bar{t}}{\bar{\rho}_p\,\bar{c}_{p_p}}\right)^{1/2}$$

This procedure insures that the explosive and piston computational layers are maintained at the appropriate thickness for accurate numerical computation.

4. Nondimensional Forms. Consider the following coordinate and variable transformations:

$$x = \frac{\bar{x} - \bar{x}_\ell}{\bar{x}_r - \bar{x}_\ell} \qquad t = \frac{\bar{u}_o}{\bar{L}_o}\,\bar{t}$$

$$F = \frac{\bar{x}_r - \bar{x}_\ell}{\bar{L}_o}$$

$$T = \bar{T}/\bar{T}_o \qquad u = \bar{u}/\bar{u}_o \qquad c_p = \bar{c}_p/\bar{R}_u$$

$$p = \frac{\bar{p}}{\bar{\rho}_o\,\bar{R}_u\,\bar{T}_o} \qquad \kappa = \frac{\bar{\kappa}}{\bar{\rho}_o\,\bar{R}_u\,\bar{u}_o\,\bar{L}_o} \qquad J = \frac{\bar{L}_o\,\bar{J}}{\bar{R}_u\,\bar{T}_o\,\bar{u}_o}$$

When introduced into equation 2 there results a nondimensional form of the heat equation.

$$\frac{\partial T}{\partial t} = \frac{1}{\rho c_p F^2} \frac{\partial}{\partial x}\left(\kappa \frac{\partial T}{\partial x}\right) + \frac{U_\ell + x\dot{F} - u}{F} \frac{\partial T}{\partial x} + \frac{a_1}{\rho c_p} \dot{p} + \frac{a_2}{c_p} J$$

where

$$U_\ell = \frac{1}{\bar{u}_o} \frac{d\bar{x}_\ell}{d\bar{t}} = \frac{\bar{U}_\ell}{\bar{u}_o}$$

$$\dot{F} = \frac{dF}{dt} = \frac{\bar{U}_r - \bar{U}_\ell}{\bar{u}_o} = U_r - U_\ell$$

The pressure relation can also be written in nondimensional form

$$m = p\, F \int_0^1 \frac{dx}{T} = pFV$$

where

$$m = \frac{\bar{R}_{air}\, \bar{T}_o}{\bar{p}_o \bar{L}_o} \bar{m}$$

The expression is solved for F with pressure and mass given,

$$F = \frac{m}{p\, V} \tag{5}$$

and for $\dot{F}$

$$\dot{F} = F\left(\frac{\dot{m}}{m} - \frac{1}{\gamma} \frac{\dot{p}}{p}\right) + \frac{W}{m\, c_p} \tag{6}$$

where

$$W = \int_0^1 \left(\kappa \frac{\partial^2 T}{\partial x^2} + \frac{\partial \kappa}{\partial x} \frac{\partial T}{\partial x}\right) \frac{dx}{T}$$

Mass variation during gap closure enters the model only through equations 5 and 6. This implies the assumption that mass is varied throughout the air layer at the local temperature such that only the volume is affected.

The nondimensional form for air thermal conductivity is

$$\kappa_{air} = C_1 T^{1/2} - C_2$$

where

$$C_1 = \frac{\bar{T}_o^{1/2}\,\bar{C}_1}{\bar{\rho}_o \bar{R}_u\,\bar{u}_o\,\bar{L}_o}$$

$$C_2 = \frac{\bar{C}_2}{\bar{\rho}_o\,\bar{R}_u\,\bar{u}_o\,\bar{L}_o}$$

The interior boundary conditions are simply

$$T_r^{n-1} = T_\ell^n \qquad n=2,3$$

$$\kappa_r^n \left(\frac{\partial T}{\partial x}\right)_r^n = \kappa_\ell^{n+1} \left(\frac{\partial T}{\partial x}\right)_\ell^{n+1} \qquad n=1,2$$

and at the exterior boundaries

left: $\quad T(t,0) = T_L(t) \quad \text{or} \quad \kappa \frac{\partial T}{\partial x}(t,0) = Q_L(t)$

right: $\quad T(t,1) = T_R(t) \quad \text{or} \quad \kappa \frac{\partial T}{\partial x}(t,1) = Q_R(t)$

The nondimensional forms of the boundary velocities are

$$U_\ell^{(1)} = \frac{-5}{2} \left(\frac{\kappa_{he}}{\rho_{he} c_{p_{he}} t}\right)^{1/2}$$

$$U_r^{(1)} = U_\ell^{(1)} = 0$$

$$U_r^{(2)} = U_\ell^{(3)} = \dot{F}^{(2)}$$

$$U_r^{(3)} = \dot{F}^{(2)} + \frac{5}{2} \left(\frac{\kappa_p}{\rho_p c_{p_p} t}\right)^{1/2}$$

5. Finite Difference Equations. The computational grid is shown in Figure 3. The coordinates of the grid points are given by

$$x_i^n = \frac{i-2}{i_{max}^n - 3} \qquad 1 \le i \le i_{max}^n$$

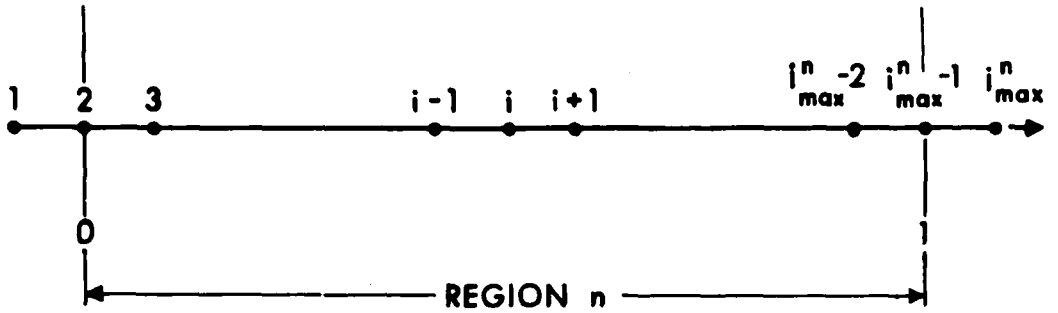

Figure 3. Computational Grid

The grid includes fictitious points on either side of each region for imposing conditions on derivatives, such that the boundary points of each region correspond to i=2 and i=i_{max}-1. The pattern for the computation of derivatives is illustrated in Figure 4. This leads to an implicit finite difference scheme for the solution of the equation. The finite difference form of the equation is applied at interior points.

$$\frac{T_i^{n\ell} - T_i^{nk}}{\Delta t} = \frac{\kappa_i^{n\ell}}{\rho_i^{n\ell} c_p^n (F^{n\ell})^2} \frac{T_{i+1}^{n\ell} - 2T_i^{n\ell} + T_{i-1}^{n\ell}}{(\Delta x^n)^2}$$

$$+ \frac{1}{\rho_i^{n\ell} c_p^n (F^{n\ell})^2} \frac{\kappa_{i+1}^{n\ell} - \kappa_{i-1}^{n\ell}}{2\Delta x^n} \frac{T_{i+1}^{n\ell} - T_{i-1}^{n\ell}}{2\Delta x^n} \qquad (7)$$

$$+ \frac{a_1^n}{\rho_i^{n\ell} c_p^n} \dot{p} + \frac{a_2^n}{c_p^n} J$$

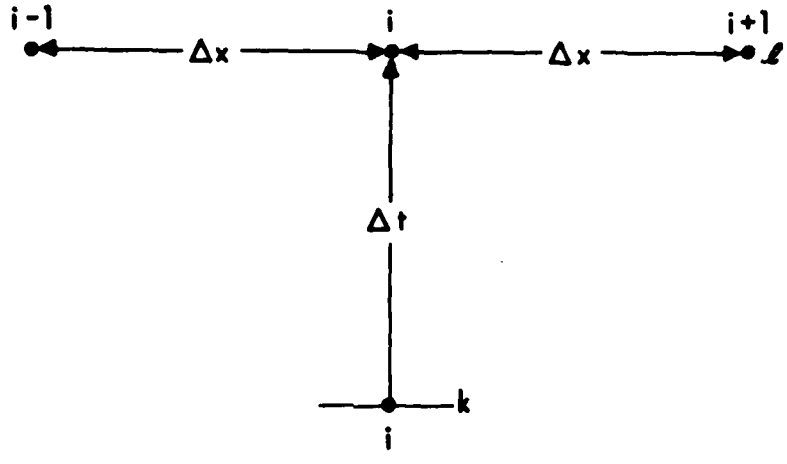

Figure 4. Derivative Pattern

The superscript ℓ refers to values at the current time step and the superscript k to values at the previous time step. The interior boundary conditions are written

$$T^{n-1}_{i_{max}-1} = T^{n}_{2} \qquad n=2,3 \tag{8}$$

$$\frac{\kappa^{n}_{i_{max}-1}}{F^{n\ell}} \quad \frac{T^{n\ell}_{i_{max}} - T^{n\ell}_{i_{max}-2}}{2\Delta x^{n}} = \frac{\kappa^{n+1}_{2}}{F^{n+1,\ell}} \quad \frac{T^{n+1,\ell}_{3} - T^{n+1,\ell}_{3}}{2\Delta x^{n+1}} \qquad n=1,2$$

and at the exterior boundaries

$$\text{left:} \quad T^{1,\ell}_{2} = T_L(t^{\ell}) \quad \text{or} \quad \frac{\kappa^{1,\ell}_{2}}{F^{1,\ell}} \frac{T^{1,\ell}_{3} - T^{1,\ell}_{1}}{2\Delta x^{(1)}} = Q_L(t^{\ell}) \tag{9}$$

$$\text{right:} \quad T^{3,\ell}_{i_{max}-1} = T_R(t^{\ell}) \quad \text{or} \quad \frac{\kappa^{3,\ell}_{i_{max}-1}}{F^{3,\ell}} \quad \frac{T^{3,\ell}_{i_{max}} - T^{3,\ell}_{i_{max}-2}}{2\Delta x^{(3)}} = Q_R(t^{\ell})$$

The total number of equations and boundary conditions is equal to the total number of unknowns.

$$N = \sum_{n=1}^{3} (i^n_{max}-2) + 6 = \sum_{n=1}^{3} i^n_{max}$$

Solutions at each time step are generated by computing F and $\dot{F}$ from equations 5 and 6 and then solving the set of simultaneous equations represented by equations 7, 8, and 9. The finite difference equations including boundary conditions must be solved in all three regions simultaneously. The solution requires the inversion of a band matrix with 3 upper and 2 lower codiagonals. This is accomplished by use of a suitable matrix inversion routine. The procedure is repeated in iterative fashion until an arbitrarily specified degree of accuracy is attained.

III. RESULTS AND DISCUSSION

A. General

The material constants for the explosive, the air and the piston are summarized in Table I. For the explosive, values for Composition-B (Comp-B) are given and for the piston those for polyethylene and steel are given. In addition to values for air, those for argon, carbon dioxide and hydrogen are included. The values of specific heat, obtained from reference 3, correspond to atmospheric pressure. The value for air applies at 1300K while those for argon, carbon dioxide, and hydrogen apply at 300K. The initial temperature of the system is always taken to be 300K.

Table I. Material Constants

	$\bar{\rho}_i$	$\bar{c}_p$	$\bar{\kappa}$	$\bar{C}_1$	$\bar{C}_2$
	kg/m^3	J/kgK	W/mK	$W/mK^{3/2}$	W/mK
Comp-B	1.69×10^{3}	1.393×10^{3}	.2623	0.	.2623
Air	1.18	1.197×10^{3}	-	2.901×10^{-3}	2.536×10^{-2}
Argon	1.62	5.23×10^{2}	-	1.743×10^{-3}	1.256×10^{-2}
Carbon Dioxide	1.80	8.23×10^{2}	-	3.236×10^{-3}	3.616×10^{-2}
Hydrogen	8.15×10^{-2}	1.42×10^{4}	-	1.928×10^{-2}	1.523×10^{-1}
Polyethylene	9.30×10^{2}	2.301×10^{3}	.4184	0.	-.4184
Steel	7.87×10^{3}	4.372×10^{2}	79.5	0.	- 79.5

When the time scale does not vary, the magnitude of the peak temperature attained at the explosive-air interface is indicative of the likelihood that a given configuration will lead to ignition. In the subsequent discussion, variations which increase this temperature are referred to as sensitizing while those that reduce it are referred to as desensitizing. In the case of the adiabatic compression model, this is the temperature achieved immediately upon piston closure. The final to initial temperature and density ratios for $\gamma = 1.4$ are plotted as functions of compression ratio in Figure 5a and the resultant interface temperatures are plotted in Figure 5b. Since the model assumes a constant thermal conductivity for air and this actually varies, upper and lower limits for the interface temperature based on the maximum and minimum values of $\bar{\kappa}$ have been computed. The maximum value occurs at the final air temperature and the minimum occurs at the interface temperature. The results indicate that increasing peak pressure is sensitizing while increasing the initial pressure is desensitizing. The latter conclusion is in conflict with the experiments. This indicates that the processes involved are not adiabatic. Further, this model does not predict sufficiently high temperatures to explain ignitions observed at the lower compression ratios

It is estimated that temperatures in excess of 650K sustained for several hundred microseconds are required for ignition of Comp-B in the activator. With initially pressurized air gaps, ignitions were observed with compression ratios as low as 600 for which the adiabatic compression interface temperature lies between 425K and 502K.

For the finite compression-rate model the heat flux was required to vanish at the exterior boundaries. The motion of these boundaries through the material results in the maintenance of a temperature very close to 300K at the left and right extremes throughout the computation. Twenty-three computational points were used in each region. The peak temperature was found to be quite sensitive to the time step and $\Delta\bar{t}=2\times10^{-8}$ was required for accuracy. A constant pressurization rate during piston closure is assumed.

$$\bar{p} = \begin{cases} \bar{p}_i \left[\left(\dfrac{\bar{p}_f}{\bar{p}_i} - 1\right)\dfrac{\bar{t}}{\bar{t}_f} + 1\right] & \bar{t} \leq \bar{t}_f \\ p_f & \bar{t}_f < \bar{t} \end{cases}$$

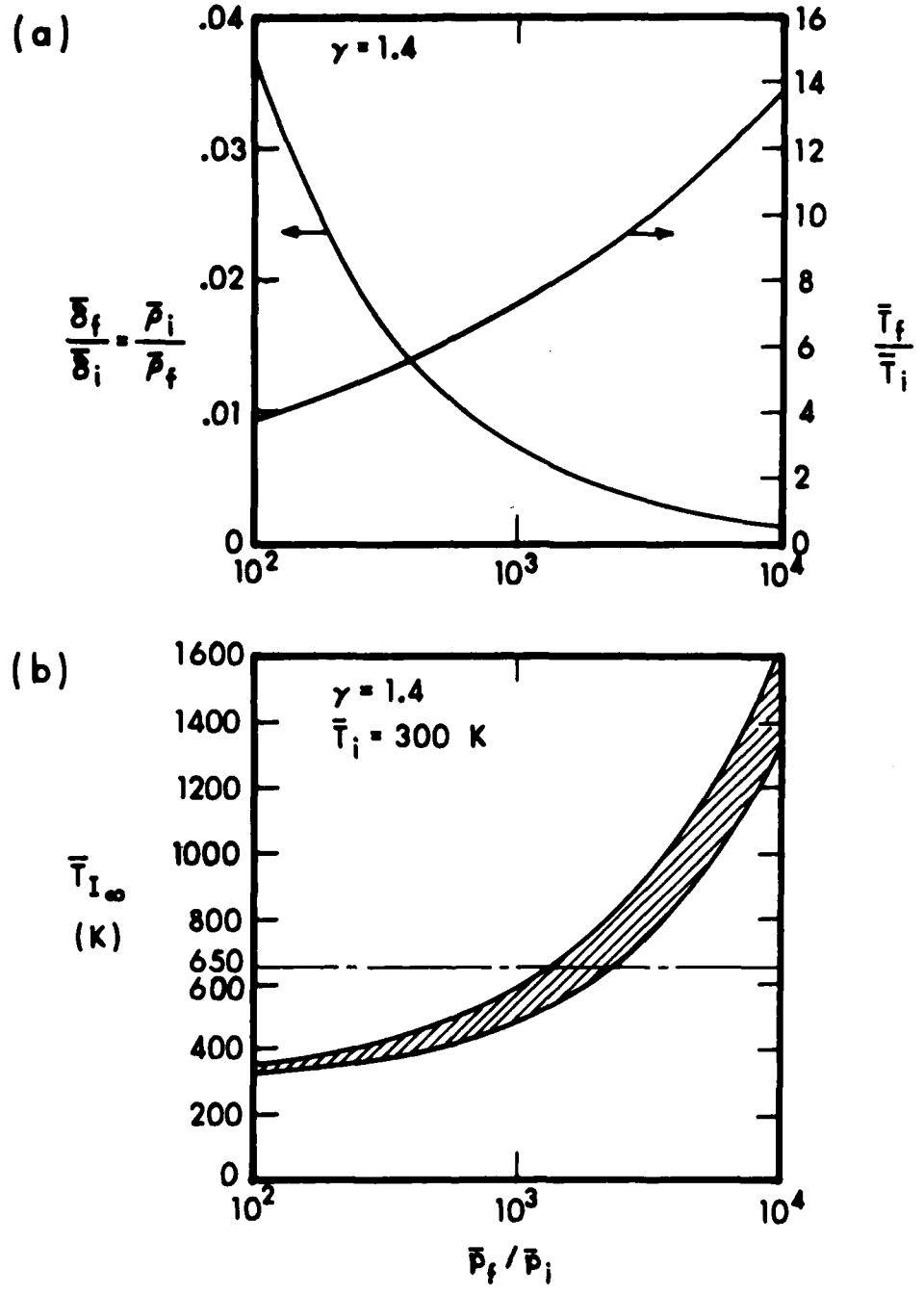

Figure 5. Adiabatic Compression Computations

A similar expression is used when there is mass variation.

$$\bar{m} = \begin{cases} \bar{m}_i \left[\left(\frac{\bar{m}}{\bar{m}_i} - 1 \right) \frac{\bar{t}}{\bar{t}_f} + 1 \right] & \bar{t} \leq \bar{t}_f \\ \bar{m}_f & \bar{t}_f < \bar{t} \end{cases}$$

where $\bar{t}_f$, the gap closure time, is 300 μs. This pressure rise time appears to be characteristic of the activator system when the total run is not equal to zero. Thus some 1.5×10^4 steps are required to reach peak pressure. Typical evolution of the temperature profile during gap closure is shown in Figure 6a and typical interface temperature and maximum air temperature histories are compared in Figure 6b. The computations are terminated shortly after the interface temperature peaks. It can be noted that the maximum air temperature is significantly higher than the interface temperature and that it peaks earlier.

B. Effects of Parameter Variations.

A number of computations were made to assess the influence of variations which were shown to affect sensitivity in the activator experiments. Specifically peak pressure and pressurization rate, initial pressure, initial gap thickness, piston material, air leakage during gap closure and the presence of alternate gases in the gap were considered. The results of this are summarized in Tables II through VII. Case B is common to all the tables and the fixed conditions for each table correspond to that case.

1. Peak Pressure and Pressurization Rate.

When a fixed value of the gap closure time is selected the peak pressure and pressurization rate are coupled. The question arises as to which of these most strongly influences peak temperature. In case A, appearing in Table II peak temperature and pressure occur simultaneously. In cases B and C the effect of heat conduction is sufficient to cause the temperature to peak and the computation to be terminated before the maximum pressure is attained. Thus, for pressurization rates in excess of 340 GPa/s and for other conditions corresponding to Table II peak temperature is a function of pressurization rate exclusively. The effect of increasing pressurization rate is sensitizing as the experiments have shown.

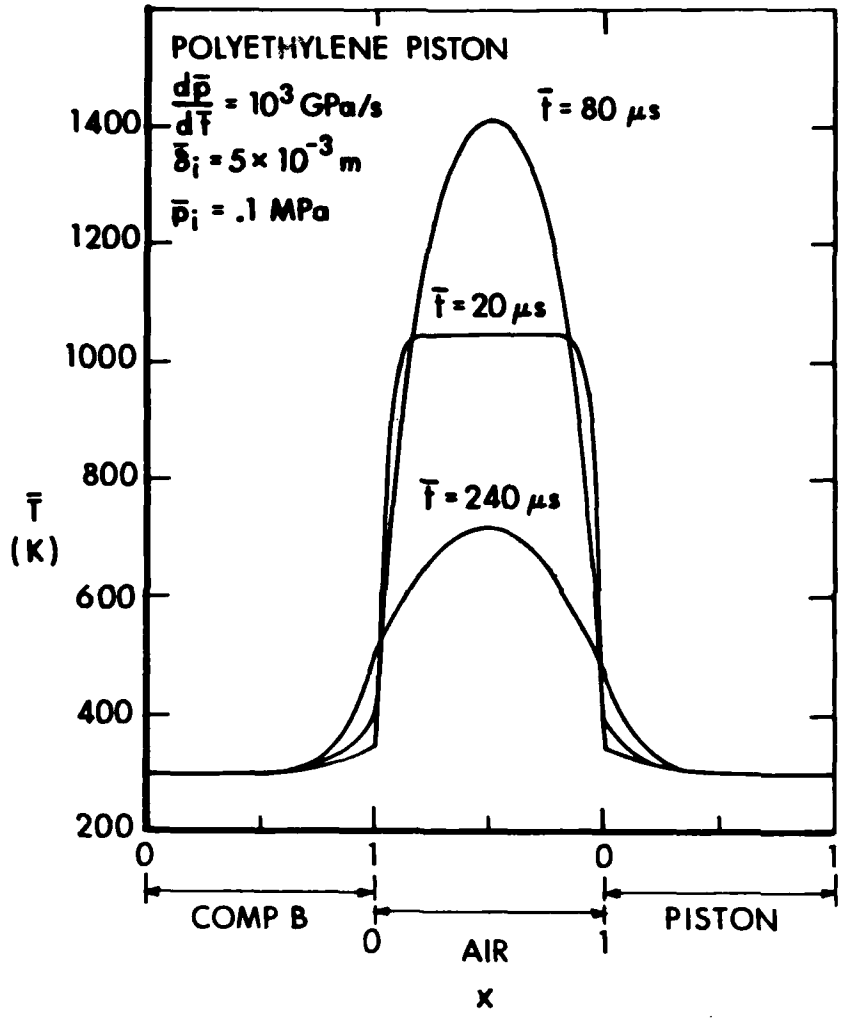

Figure 6a. Typical Temperature Profiles

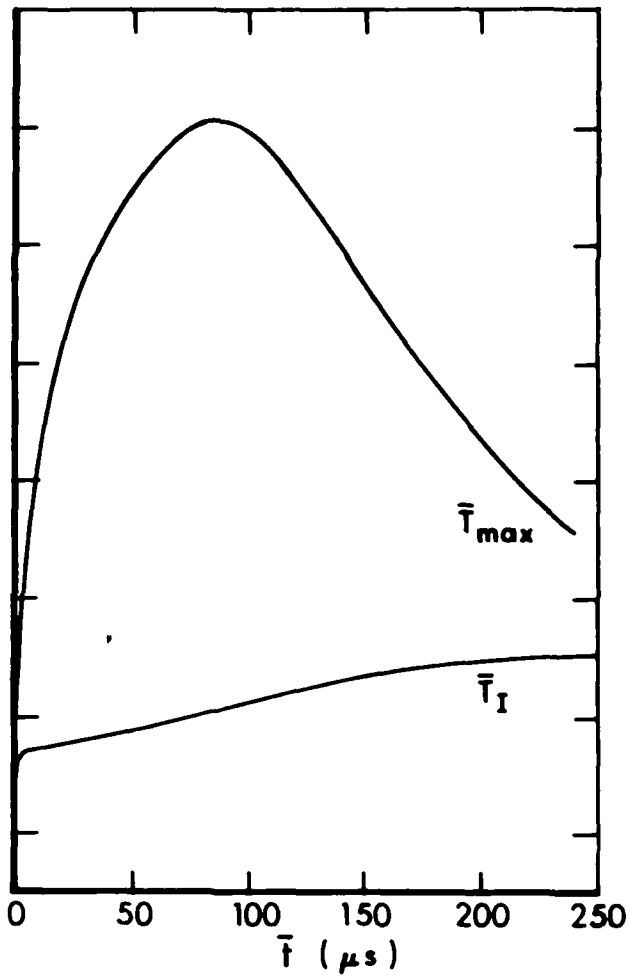

b. Typical Temperature History

Table II. Effects of Pressurization Rate

Case	Peak Pressure	Pressurization Rate	Pressure at Peak Temperature	Peak Interface Temperature
	GPa	GPa	GPa	K
A	.1	3.4×10^{2}	.10	432
B	.3	1.0×10^{3}	.25	512
C	1.0	3.4×10^{3}	.47	613

2. Initial Pressure.

As initial pressure is increased the effect is at first sensitizing but subsequently desensitizing. The adiabatic compression model predicted only the desensitization while in the experiments only the sensitizing effect was observed. The transition begins approximately where peak pressure is achieved. This suggests that the experiments lie in the regime in which sensitivity is determined by pressurization rate.

Table III. Effects of Initial Pressure

Case	Initial Pressure	Mass of Air in Gap	Pressure at Peak Temperature	Peak Interface Temperature
	MPa	kg/m^2	GPa	K
B	.10	5.89×10^{-3}	.25	512
D	.15	8.83×10^{-3}	.30	549
E	.20	1.18×10^{-2}	.30	555
F	.30	1.77×10^{-2}	.30	543

3. Inital Gap Thickness.

Increasing the initial gap is also sensitizing, as observed experimentally. Cases D and H may be compared to show that increasing the initial gap thickness is still sensitizing when the mass of air in the gap is held constant.

Table IV. Effects of Initial Gap Thickness

Case	Initial Gap Thickness	Mass of Air in Gap	Peak Interface Temperature
	m	kg/m^2	K
G	2.5×10^{-3}	2.94×10^{-3}	428
B	5.0×10^{-3}	5.89×10^{-3}	512
H	7.5×10^{-3}	8.83×10^{-3}	573

4. Piston Material.

Increasing the thermal diffusivity ($\bar{\kappa}_i/\bar{\rho}_i\ \bar{c}_p$) of the piston by substituting steel for polyethylene is only mildly desensitizing.

Table V. Effects of Piston Material

Case	Material	Thermal Diffusivity	Peak Interface Temperature
		Wm^2/J	K
B	Polyethylene	1.96×10^{-7}	512
I	Steel	2.31×10^{-5}	505

5. Leakage.

The leakage of fifty percent of the air during gap closure is desensitizing. The experiments indicate that using a tightly fitting piston increases sensitivity.

Table VI. Effects of Leakage

Case	$\bar{m}_f/\bar{m}_i$	Pressure at Peak Temperature	Peak Temperature
		GPa	K
B	1.0	.19	512
J	0.5	.25	494

6. Alternate Gases.

Gases other than air have been substituted by some experimenters[4] in order to test the compressive heating hypothesis. In general the results have been inconclusive. Here computations have been made for argon, carbon dioxide and hydrogen. Results from the adiabatic compression model are given in Figure 7, where only the lower value of the interface temperature, based on the interface value of $\bar{\kappa}$, has been plotted. This model predicts a significant difference in the pressure required for ignition with different gases. The results of finite compression-rate model computations are presented in order of increasing sensitivity in Table VII. The order of sensitivity is the same for both models. Argon has the highest ratio of specific heats and produces the hottest gas on compression. However, since it possesses the smallest heating efficiency of the four gases it transfers the smallest percentage of its temperature increase to the explosive and only ranks second in sensitivity. The high heating efficiency of hydrogen causes the adiabatic compression model to predict a sensitivity significantly higher than for the other gases while the finite compression-rate model shows only a very slightly higher sensitivity. Note that the high thermal diffusivity of hydrogen causes the temperature to peak at a much earlier point in the compression when the gas temperature is lower.

Table VII. Effects of Alternate Gases

Gas	γ	Thermal Diffusivity	Heating Efficiency	Pressure at Peak Temperature	Peak Temperature
		Wm^2/J		GPa	K
CO_2	1.31	1.34×10^{-5}	4.77×10^{-5}	.26	490
Air	1.40	1.76×10^{-5}	5.70×10^{-5}	.25	512
Argon	1.67	2.08×10^{-5}	2.42×10^{-5}	.28	628
H_2	1.41	1.57×10^{-4}	3.40×10^{-4}	.09	632

C. Validity of the One-Dimensional Models

The time to explosion for the activator experiments is judged to be within a few hundred microseconds of the time at which peak temperature is reached. By using kinetic parameters for RDX it is possible to roughly estimate that sustained temperatures in excess of 650K are required for

[4] *Arthur D. Little, Inc., "Cavity Standards for Cast-Loaded Artillery Projectiles", Revised Final Report for Picatinny Arsenal, 30 Mar 57.*

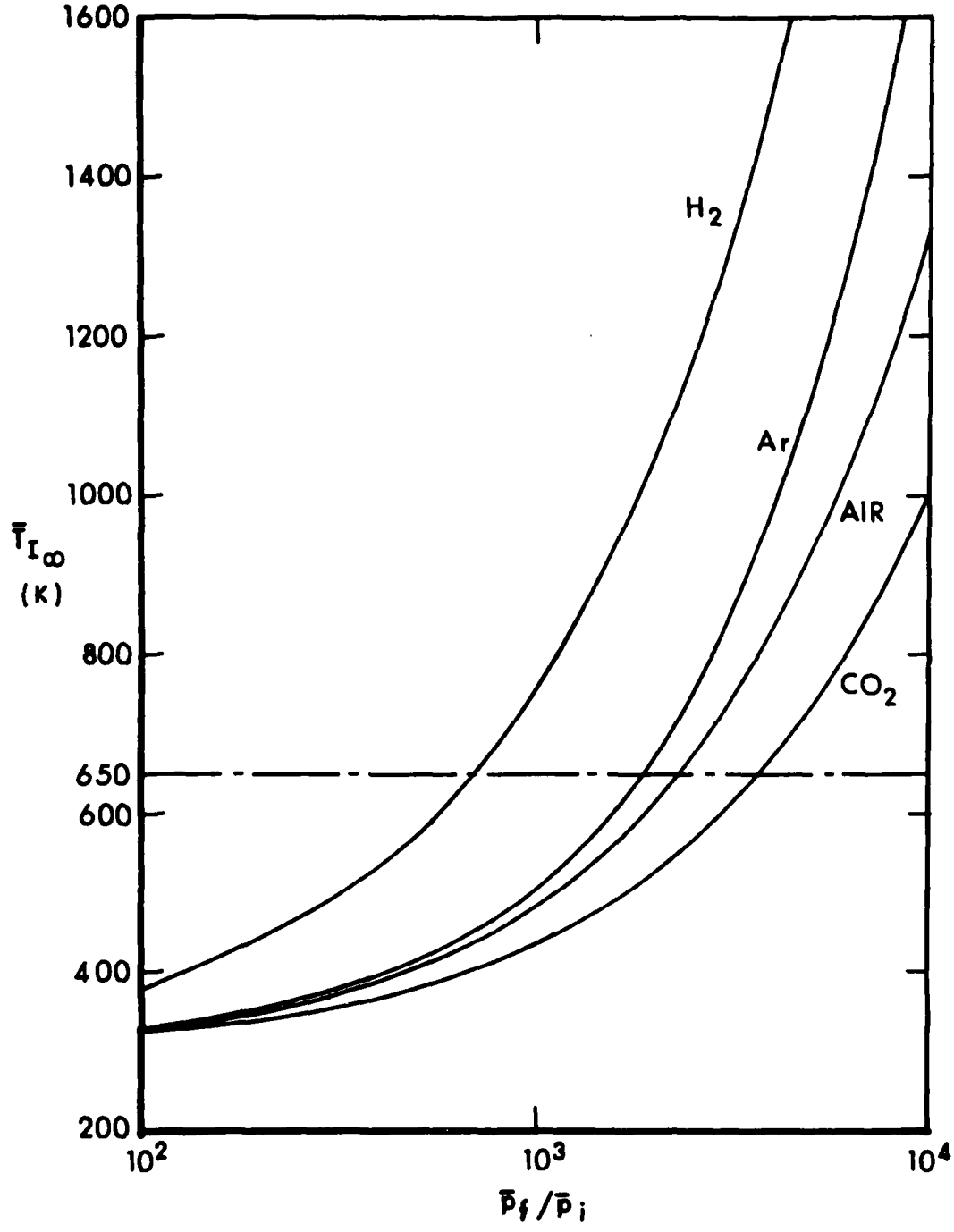

Figure 7. Adiabatic Compression of Alternate Gases

ignition on this time scale. The adiabatic compression model predicts the highest possible values of the explosive-air interface temperature. Reference to Figure 5a indicates that sufficiently high temperatures can only be produced at compression ratios higher than many at which ignition was observed. In addition, at finite pressurization rates even lower temperatures are predicted and in no case can observed ignitions be accounted for. The situation is further aggravated by the fact that air leakage in the activator renders the environment even less hostile. This discrepancy between the predictions and the experiments arises because the one-dimensional planar gap model is not strictly valid. Among the multidimensional effects that may come into play are:

1. enhanced energy transport
2. rapid pressurization
3. convergent air flow
4. dieseling

In order to critically examine how these influence sensitivity it is necessary to introduce them into the one-dimensional scheme.

1. Enhanced Energy Transport. One of the assumptions of the analysis is that thermal conductivity is the only mechanism of energy transport through the air layer. If turbulence develops in the air layer, this will enhance energy transport and may serve to increase the interface temperature. This effect may be readily introduced into the present models by assuming that the air possesses an effective thermal conductivity which is greater than the actual value. This is reflected through the value of α_i in equation 1 and is introduced into the finite compression rate model[1] by specifying a thermal conductivity multiplier, σ, defined as the ratio of the effective to the actual conductivity. Of the multidimensional effects considered, only enhanced energy transport serves to increase the theoretical maximum temperature of the adiabatic compression model defined by equation 1. Neither pressurization rate nor degree of convergence can be varied so as to produce higher temperatures than this during finite rate compressions. Included in Figure 8 is a plot of theoretical maximum interface temperature versus the thermal conductivity multiplier for a pressure ratio of 3×10^3. The temperature varies between the limits of initial temperature, $\bar{T}_i$, for $\alpha_i=0$ and final air temperature, $\bar{T}_i(\bar{p}_f/\bar{p}_i)^{\frac{\gamma-1}{\gamma}}$, for $\alpha_i\to\infty$. Thus the interface temperature becomes increasingly sensitive to compression ratio with increasing thermal conductivity.

When the finite compression-rate model is used different results are obtained depending on the variation of energy transport enhancement through the air layer. The expression used for σ is

$$\sigma = (\sigma_{max}-1)\ (1-x)^s + 1$$

When s=0 the thermal conductivity is augmented by the factor σ_{max} uniformly throughout the air layer. For larger values of s the effect is concentrated nearer to the explosive surface as in a boundary layer. This is illustrated in the inset in Figure 8 where the explosive lies at x=0 in the air layer. If there are no boundary effects only a very limited increase in temperature results from enhanced energy transport as illustrated in Figure 8 for s=0. The temperature remained below 650K for values of σ_{max} throught 10^6. The reason that this occurs is more clearly illustrated in Table VIII. As σ_{max} is increased, peak temperature occurs at increasingly early times during the compression since the thermal conductivity increases while the rate of heat generation from pressurization remains unchanged. The interface temperature is then limited by total energy availible in pressurizing the air to increasingly lower pressures. Thus, in the absence of boundary effects, enhanced energy transport is ineffective in increasing the temperature prediction unless the conditions of adiabatic compression are simultaneously approached. This may be accomplished through rapid pressurization or convergence. With concentrated energy transport enhancement (s>0) it is possible to predict temperatures high enough to explain ignition. with values of σ_{max} less than ten as illustrated in Figure 8 for s=1,2 and 5.

Table VIII. Effects of Energy Transport (s=0)

σ_{max}	Pressure at Peak Temperature	Peak Temperature
	GPa	K
1	.25	512
10^2	.08	571
10	.04	607
10^3	.04	609
10^4	.04	611
10^5	.04	614
10^6	.04	615

2. Rapid Pressurization.

Since uniformly increased thermal conductivity favorably affects the results of the adiabatic compression model but not the results of its

nonadiabatic counterpart, it is of interest to consider an effect which causes the finite compression-rate model to approach the adiabatic compression limit. This occurs as the pressurization rate becomes arbitrarily large and can be introduced into the finite compression-rate model by specifying the pressurization rate independent of the peak pressure when making the computation. This has the desired effect on the interface temperature prediction as illustrated in Figure 9 for $\sigma = \sigma_{max} = 10$. These computations were made with the time step reduced in inverse proportion to the pressurization rate. The temperature approaches the adiabatic limit with increasing pressurization rate. The computations could not be carried to higher pressurization rates without a significant loss of accuracy since an increasingly small region of the air layer is affected by heat conduction. Temperatures sufficiently high to explain ignition are obtained by increasing the pressurization rate by a factor less than ten.

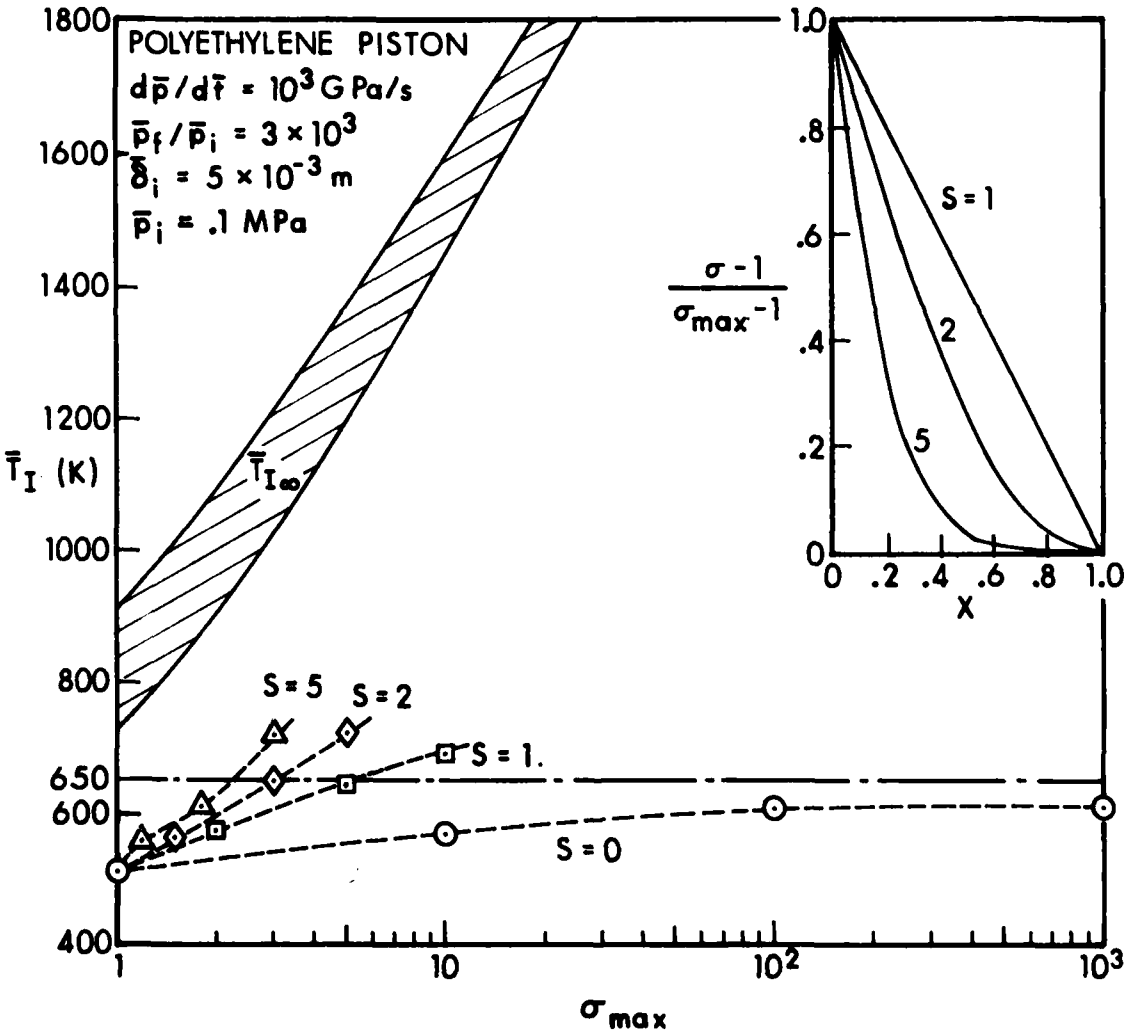

Figure 8. Effect of Energy Transport on Interface Temperature

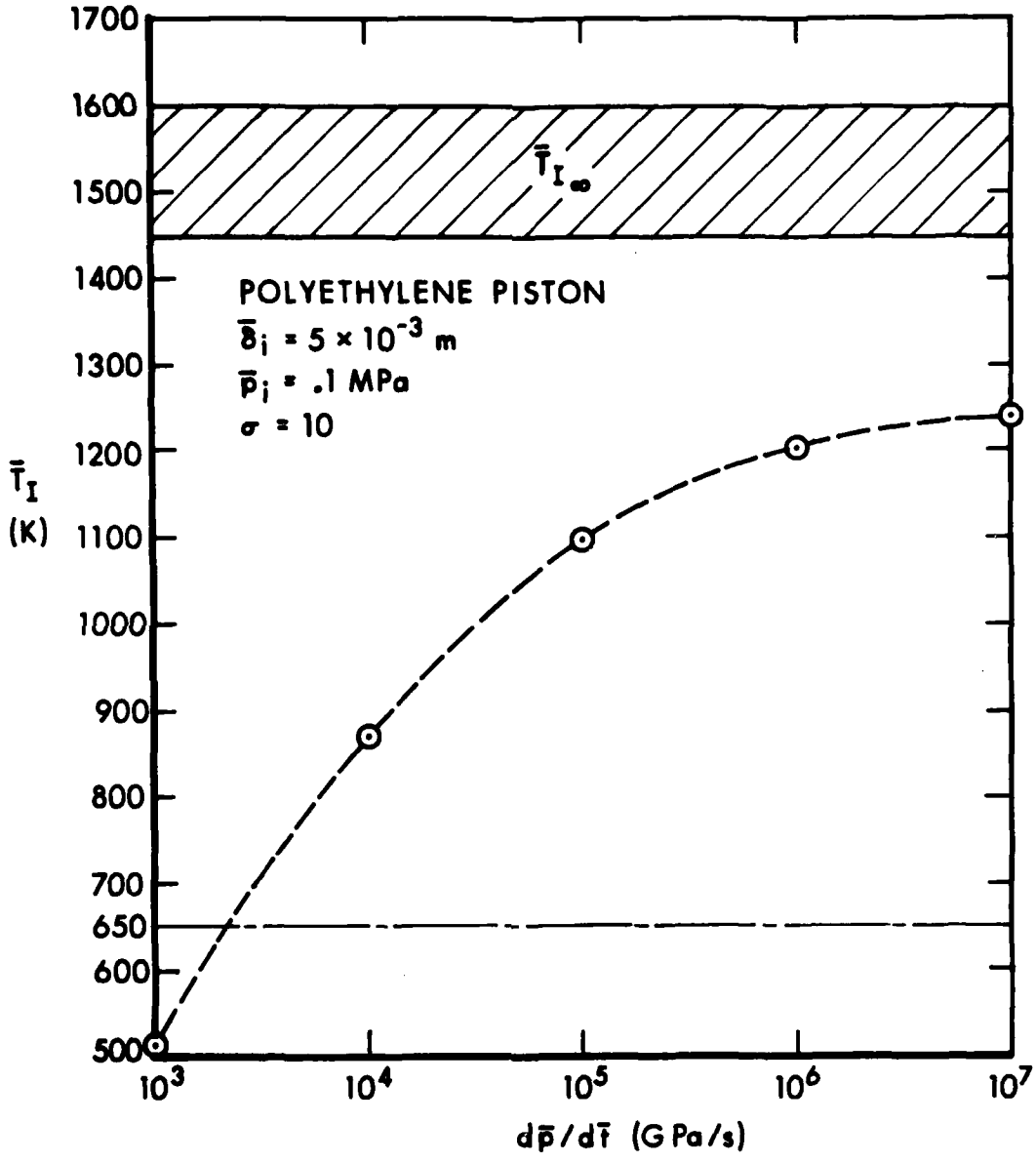

Figure 9. Effect of Pressurization Rate on Interface Temperature

3. Convergent Air Flow. Reference to Figure 5a indicates that for pressures in the range of interest a gap initially 5mm thick will compress to as small as 10μm. This is smaller than the typical explosive particle size and than the surface irregularities in the explosive sample. On the scale of its final thickness, then, the gap may not be regarded as planar. During the final portion of gap closure air will flow from regions in which the explosive protrudes above its mean surface elevation into surface defects. This is illustrated schematically in Figure 10. Geometrically, the problem retains its one-dimensional character only on a local scale in cylinders whose dimensions are small compared to dimensions over which significant variation in the surface elevation occurs. As the piston is closed air crosses these cylinder boundaries. Thus, the mass of the air residing in the final local gap differs from that in the original cylinder. Attempts to model the effects of defects of various sizes showed that the defect size alone was not an important determinant of peak interface temperature but that only local mass addition was effective in increasing the temperature. This is related to the defect size in some unknown manner. Thus, the mass addition which occurs at surface defects may be introduced into the one-dimensional model by simply specifying the final to initial mass ratio $\bar{m}_f/\bar{m}_i$ and assuming a linear variation during gap closure. These results are

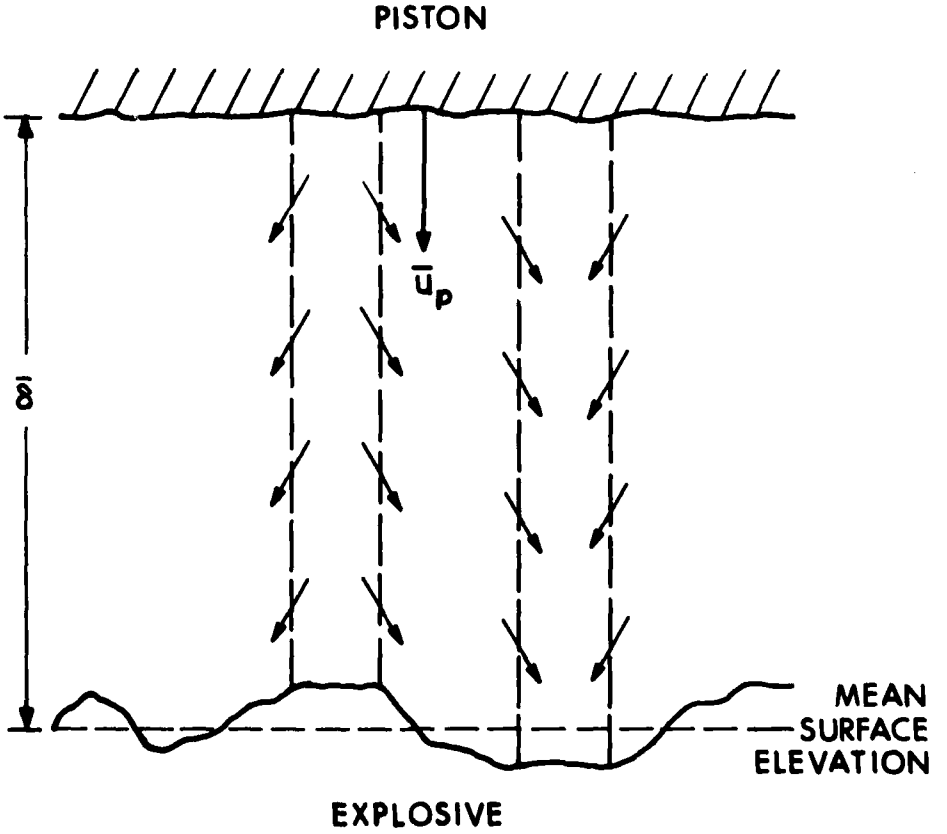

Figure 10. Schematic of Convergence Effect

summarized in Figure 11 for $\sigma = \sigma_{max} = 10$ (since in the absence of boundary effects convergence alone cannot cause the interface temperature to exceed the adiabatic compression limit). This also increases the temperature prediction enough to explain ignition.

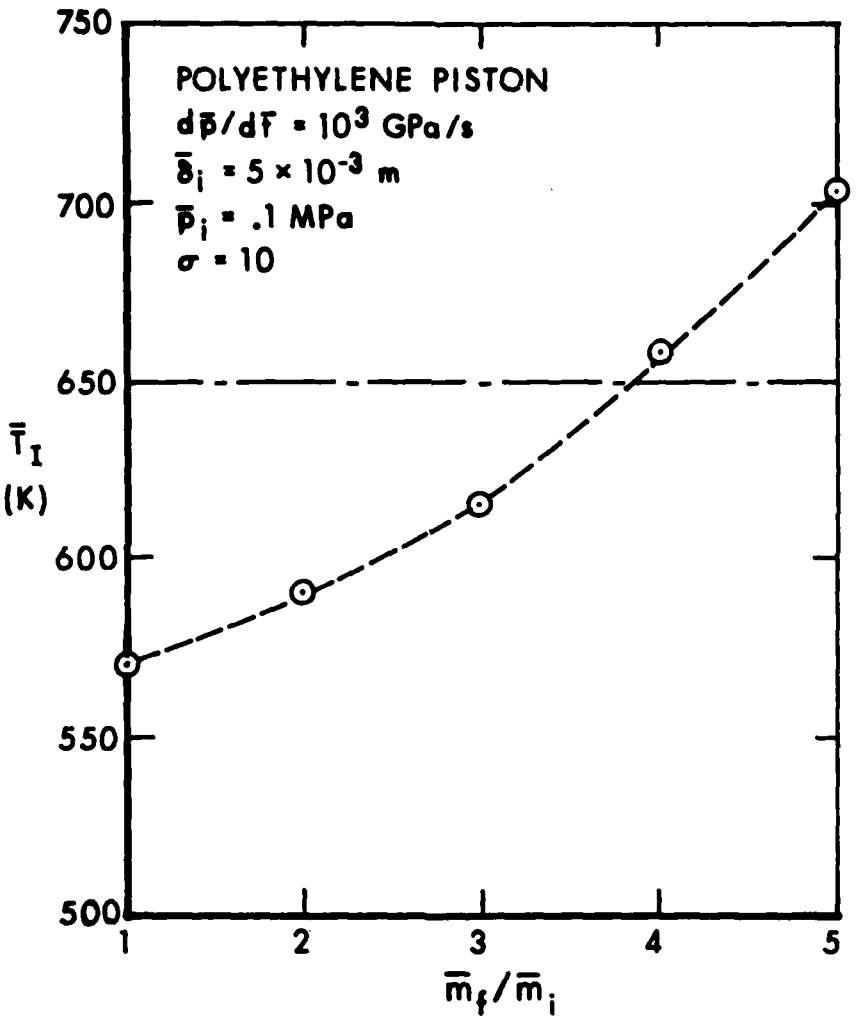

Figure 11. Effect of Convergence on Interface Temperature

4. Combined Effects. A single case was considered to demonstrate the combined effects of concentrated energy transport enhancement, rapid pressurization and convergent air flow. Relatively mild values of the

parameters describing these effects were chosen as follows:

$$\sigma_{max} = 2$$

$$s = 1$$

$$\frac{d\bar{p}}{d\bar{t}} = 2 \times 10^3 \text{ GPa/s}$$

$$\frac{\bar{m}_f}{\bar{m}_i} = 1.5$$

The initial conditions are those corresponding to case B. The resulting maximum interface temperature was 668K.

5. Dieseling. If fine particles of explosive protrude or are entrained into the air, the temperature at the surface of the particles will exceed the planar interface temperature when the particles are sufficiently small. The Comp-B heated layer thickness given by equation 4 is a measure of the particle size required to yield this effect. This thickness is plotted as a function of time in Figure 12. Times range between 10 μs and 10 ms. The maximum time for events observed in the activator is approximately 1 ms which corresponds to a heated layer thickness of about 30 μm. This may be interpreted to mean that particles whose radius is less than 30 μm exhibit a surface temperature higher than that associated with a semi-infinite layer. It is reasonable to believe that particles of this size may be present and to conclude that dieseling as a sensitizing mechanism may not be ruled out.

IV. CONCLUSION

Two analytical models to predict the temperature history of an explosive-air interface under conditions of compressive heating have been reported herein. The adiabatic compression model is inadequate to describe the activator experiments since it excludes effects of pressurization rate, gap thickness, piston properties and mass addition or leakage, and improperly describes the effect of initial pressure. The finite compression-rate model, on the other hand, yields qualitative agreement with the activator experiments with respect to all of the above stimulus variations. In addition, computations for the alternate gases - argon, carbon dioxide and hydrogon - show similar effects on sensitivity using both models. The most important observation, however, is that this planar one-dimensional model does not explain ignition. This may indicate that multidimensional processes are important in the experiments. Several such processes have been identified and introduced into the models. The most important of these is turbulence in the

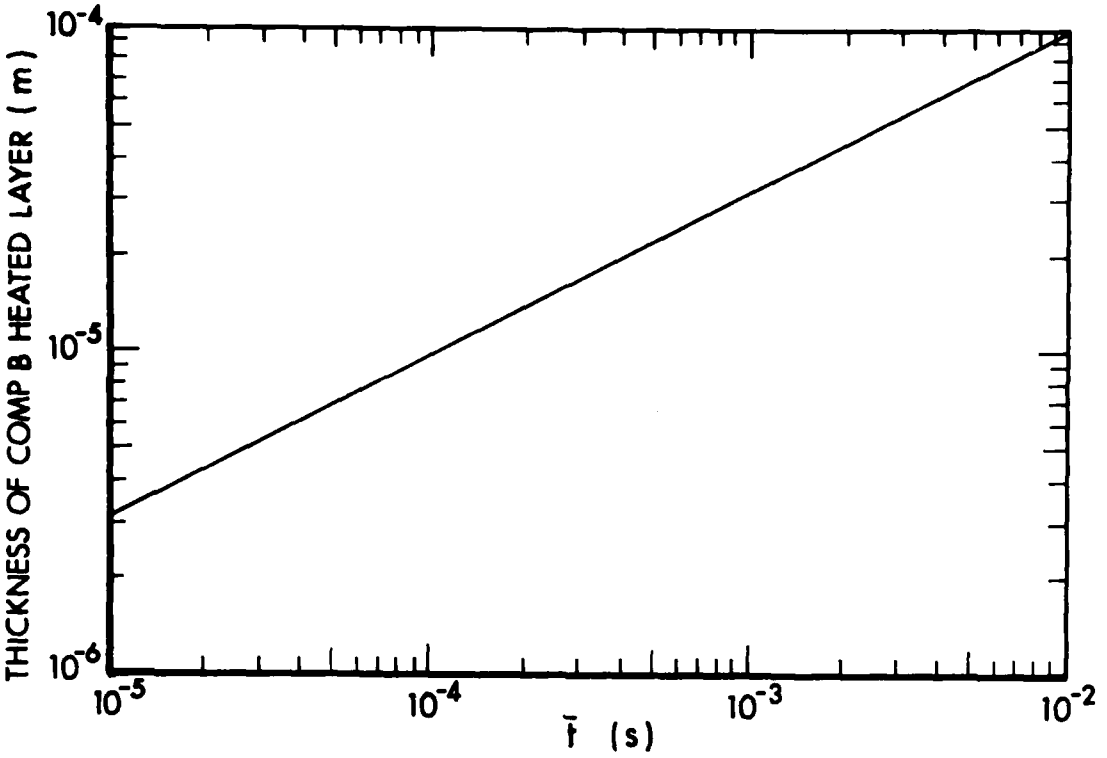

Figure 12. Comp-B Heated Layer Thickness

air which serves to enhance the energy transport to the interface. This effect is required to increase the theoretical maximum temperature which is otherwise too low. The finite compression-rate model results show that enhanced energy transport alone still does not explain ignition unless the effect is concentrated near the explosive-air interface. A combination of this effect with either rapid pressurization or convergent airflow is necessary when no such boundary effects exist. A combination of these effects will produce temperatures high enough to explain ignition with relatively mild deviation of each influencing factor from the one-dimensional planar value. Finally, the dieseling mechanism of sensitization has been discussed. The particle size required for entrained particles to show higher surface temperatures in the time frame of events in the activator is within the range of those which are actually present in the explosive charge. These conclusions are subject to the limitations of the model.

APPENDIX

The flow of the gas during gap closure should satisfy both the equations of continuity and conservation of momentum. In nondimensional form these are

$$\frac{\partial \rho}{\partial t} = \frac{U_\ell + x\dot{F} - u}{F} \frac{\partial \rho}{\partial x} - \frac{\rho}{F} \frac{\partial u}{\partial x}$$

$$\frac{\partial u}{\partial t} = \frac{U_\ell + x\dot{F} - u}{F} \frac{\partial u}{\partial x} + \frac{4}{3\rho F^2} \mu \frac{\partial^2 u}{\partial x^2} - \frac{1}{\rho F} \frac{\partial p}{\partial x}$$

However, they are supplanted in the present model by the assumptions of linear velocity variation and uniform pressure. It is of interest to examine the conditions under which these assumptions satisfy continuity and conservation of momentum.

The linear velocity variation is written

$$u = xu_p = U_\ell + x\dot{F}$$

so that

$$U_\ell + x\dot{F} - u = 0 ,$$

$$\frac{\partial u}{\partial x} = u_p = \dot{F} ,$$

$$\frac{\partial^2 u}{\partial x^2} = 0 ,$$

and

$$\frac{\partial u}{\partial t} = x\ddot{F}$$

since $U_\ell = 0$ for the gap. With these expressions, the continuity equation becomes

$$\frac{1}{\rho}\frac{\partial \rho}{\partial t} = \frac{-\dot{F}}{F}$$

Since the right hand side is a function of t only, density variations with x must be negligible and

$$\frac{d\rho}{\rho} = \frac{-dF}{F}$$

or the density varies inversely as the gap thickness.

Since pressure is uniform, $\frac{\partial p}{\partial x} = 0$ and the momentum equation may be written

$$\ddot{xF} = 0$$

This implies that the piston acceleration must be negligible.

NOMENCLATURE

$\bar{c}_p$	specific heat at constant pressure
F	nondimensional layer thickness
i	grid point index
$\bar{J}$	heat produced by chemical reaction
$\bar{L}_o$	reference length
$\bar{m}$	mass per unit area
$\bar{p}$	pressure
$\bar{Q}$	heat flux per unit area
$\bar{R}$	gas constant
$\bar{R}_u$	universal gas constant
$\bar{T}$	temperature
$\bar{t}$	time
$\bar{U}$	boundary velocity
$\bar{u}$	particle velocity
$\bar{x}$	distance
β	heating efficency
$\bar{\delta}$	layer thickness
γ	ratio of specific heats, $\bar{c}_p$ / $\bar{c}_v$
$\bar{\kappa}$	thermal conductivity
$\bar{\rho}$	density
σ	thermal conductivity multiplier
$\bar{\mu}$	viscosity

SUBSCRIPTS

air	value of constant for air
f	value after piston closure
he	value of constant for explosive
I	value at explosive air interface
i	value at initial state
ℓ	left end of region
o	reference value
p	value for piston
r	right end of region
∞	theoretical maximum value

SUPERSCRIPTS

k	previous time step
ℓ	present time step
n	region index
–	dimensional parameter
.	derivative with respect to t

DISTRIBUTION LIST

No. of Copies	Organization
12	Commander Defense Technical Info Center ATTN: DDC-DDA Cameron Station Alexandria, VA 22314
1	Commander US Army Materiel Development and Readiness Command ATTN: DRCDMD-ST 5001 Eisenhower Avenue Alexandria, VA 22333
10	Commander US Army Armament Research and Development Command ATTN: DRDAR-TSS (2 cys) DRDAR-LC/J. Frasier DRDAR-LCA/J. Hershkowitz DRDAR-LCE/D. Wiegand DRDAR-LCE/W. Voreck DRDAR-LCE/P. Marinkas DRDAR-LCM/L. Saffian DRDAR-LCM-E/S. Kaplowitz DRDAR-LCE/R. Walker Dover, NJ 07801
3	Commander US Army Armament Materiel Readiness Command ATTN: DRSAR-LEP-, Tech Lib DRSAR-LC/L. Ambrosini DRSAR-LEM/R. Zastrow Rock Island, IL 61299
1	Commander US Army Aviation Research and Development Command ATTN: DRSAV-E P.O. Box 209 St. Louis, MO 63166

No. of Copies	Orgainzation
1	Director US Army Air Mobility Research and Development Laboratory Ames Research Center Moffett Field, CA 94035
1	Commander US Army Communications Research and Development Command ATTN: DRDCO-PPA-SA Fort Monmouth, NJ 07703
1	Commander US Army Electronics Research and Development Command Technical Support Activity ATTN: DELSD-L Fort Monmouth, NJ 07703
2	Commander US Army Missile Research and Development Command ATTN: DRDMI-R DRDMI-YDL Redstone Arsenal, AL 35809
1	Commander US Army Tank Automotive Research & Development Cmd ATTN: DRDTA-UL Warren, MI 48090
1	Director US Army TRADOC Systems Analysis Activity ATTN: ATAA-SL, Tech Lib White Sands Missile Range NM 88002
2	Commander Naval Surface Weapons Center ATTN: L. Roslund D. Price Silver Spring, MD 20910

DISTRIBUTION LIST (Continued)

No. of Copies — Organization

3 Commander
Naval Weapons Center
ATTN: Bud Sewell
Taylor Joyner
Jack Pakulak
China Lake, CA 93555

1 Commander
Naval Weapons Station
NEDED
ATTN: L. Rothstein
Yorktown, VA 23691

1 AFATL/DLDE
ATTN: Dr. C. McCullough
Eglin AFB, FL 32542

1 Director
Lawrence Livermore Laboratory
ATTN: Milton Finger
P.O. Box 808
Livermore, CA 94550

1 Director
Lawrence Livermore Laboratory
ATTN: Edward Lee
P.O. Box 808
Livermore, CA 94550

1 Director
Lawrence Livermore Laboratory
ATTN: Raymond McQuire
P.O. Box 808
Livermore, CA 94550

1 Director
Lawrence Livermore Laboratory
ATTN: S. Sadic
P.O. Box 808
Livermore, CA 94550

No. of Copies — Organization

1 Director
Los Alamos Scientific Laboratory
University of California
ATTN: B. G. Craig
P.O. Box 1663
Los Alamos, NM 87545

1 Director
Los Alamos Scientific Laboratory
University of California
ATTN: C. Mader
P.O. Box 1663
Los Alamos, NM 87545

1 Princeton Combustion Research Labs, Inc.
ATTN: M. Summerfield
1041 U. S. Hwy 1 N.
Princeton, NJ 08540

1 Hoffman-La Roche, Inc.
Corporate Engineering Dept
ATTN: S. Grossel
Nutley, NY 07110

1 SRI International
ATTN: Michael Cowperthwaite
333 Ravenswood Avenue
Menlo Park, CA 94025

Aberdeen Proving Ground

Dir, USAMSAA
ATTN: DRXSY-D
DRXSY-MP, H. Cohen
Cdr, USATECOM
ATTN: DRSTE-TO-F
Dir, Wpns Sys Concepts Team,
Bldg. E3516, EA
ATTN: DRDAR-ACW

USER EVALUATION OF REPORT

Please take a few minutes to answer the questions below; tear out this sheet and return it to Director, US Army Ballistic Research Laboratory, ARRADCOM, ATTN: DRDAR-TSB, Aberdeen Proving Ground, Maryland 21005. Your comments will provide us with information for improving future reports.

1. BRL Report Number _____

2. Does this report satisfy a need? (Comment on purpose, related project, or other area of interest for which report will be used.)

_____

_____

_____

3. How, specifically, is the report being used? (Information source, design data or procedure, management procedure, source of ideas, etc.) _____

_____

_____

4. Has the information in this report led to any quantitative savings as far as man-hours/contract dollars saved, operating costs avoided, efficiencies achieved, etc.? If so, please elaborate.

_____

_____

5. General Comments (Indicate what you think should be changed to make this report and future reports of this type more responsive to your needs, more usable, improve readability, etc.) _____

_____

_____

_____

6. If you would like to be contacted by the personnel who prepared this report to raise specific questions or discuss the topic, please fill in the following information.

Name: _____

Telephone Number: _____

Organization Address: _____

_____

_____